Elastic properties of two-component grouts at short curing times: The role of bentonite

Tunnelling and Underground Space Technology 130 (2022) 104756

Contents lists available at ScienceDirect

Tunnelling and Underground Space Technology incorporating Trenchless Technology Research

journal homepage: www.elsevier.com/locate/tust

Elastic properties of two-component grouts at short curing times: The role of bentonite

Carmine Todaro [a,*], Francesca Pace [b]

[a] Institute of Geosciences and Earth Resources (IGG), Consiglio Nazionale delle Ricerche, sede di Torino Politecnico, Corso Duca degli Abruzzi 24, 10129 Torino, Italy
[b] Department of Environment, Land and Infrastructure Engineering (DIATI), Politecnico di Torino, Corso Duca degli Abruzzi 24, 10129 Torino, Italy.

A B S T R A C T

Two-component grout is nowadays the material most used for the backfilling phase in tunnelling with a shield machine. The operative simplicity of the technology and the fast hardening reaction between the two components are the main reasons that have contributed to the intensive spread of the use of this backfilling technique all around the world. Although bentonite is one of the basic ingredients for the grout production, its effect on the elastic properties of the grout has not been completely investigated so far. In this work, six different two-component grouts and their elastic properties have been studied by means of geophysical measurements. The six grouts were characterised by the same mix design and five different bentonites, while one grout had no bentonite. The variation of the dynamic parameters over time was analysed at short curing times (up to 24 h). In detail, the shear wave velocity, the dynamic moduli and Poisson's ratio were determined by means of the ultrasonic pulse velocity technique. The results show that the grouts with the bentonites have higher dynamic moduli than the grout without the bentonite. Moreover, a final analysis of the experimental data provided an analytical relationship to calculate the shear-wave velocity for each of the six grouts at any curing times.

1. Introduction

Shielded machines are nowadays the machines most commonly used in tunnelling. The difference between the diameter of the head of the machine and of the extrados of the assembled lining is expressly designed in order to avoid the machine locking, on the one hand, and to permit the assembly of linings under the shield protection on the other. The creation of this gap, which is referred to as the annulus, is essential (Wan et al., 2021). As reported by Thewes and Budach (2009), the annulus commonly ranges between 13 and 18 cm and it is determined by four different factors: the overcutting tools (located circumferentially on the head to produce a bored diameter slightly larger than that of the machine), the shield conicity, the shield thickness, and the depth of the tail brushes (the main mechanical component that forms the sealing system together with the grease).

The annulus must be continuously filled and the backfilling phase occurs at the same time as the machine is advancing. Different technologies can be used for backfilling (EFNARC, 2005; Pellegrini and Perruzza, 2009). To date, two-component grout is the most commonly used backfilling technique because it is characterised by the fastest hardening reaction among the existing alternatives (Boscaro et al., 2015; Peila et al., 2011). This singular property guarantees the locking of segments in the designed position and prevents surface settlements (Oggeri et al., 2022). Furthermore, after just 1 h of curing, two-component grout exhibits enough strength to bear the backup load and to distribute a possible punctual load to a higher surface, thanks to its ability to create a uniform layer between the linings and the ground (Ivantchev and Del Rio, 2015; Shah et al., 2018). Despite the worldwide spread of the technology (Todaro et al., 2020a; 2022b), not all of its aspects have been completely studied. For example, considering the ingredients used for grout preparation, the role of bentonite is still unclear. It is used to increase the waterproofing capacity of the hardened grout, but it also helps in the gelation phase (Pelizza et al., 2010; Pelizza et al., 2011; Peila et al., 2011). Even though its fundamental role in mortar stabilisation or in the sealing material in borehole applications is well known (Mesboua et al., 2018; Viccario, 2018), its involvement in the strength at short curing times has only recently been investigated (Todaro et al., 2022c). At this point of the investigation, speculating on a sort of parallelism with standard mortars, a scientific question arises: could the bentonite also be involved in the elastic properties of the two-component grout? Indeed, it should be reported that currently the Young's modulus (and to a slightly lesser degree also the shear modulus and the Poisson's ratio) is becoming the most important mechanical parameter for the characterisation of two-component grouts. This parameter is in fact required first by designers during the project and then during the construction phases to verify the compliance of a given

* Corresponding author at: IGG, Consiglio Nazionale delle Ricerche, sede di Torino Politecnico, DIATI, corso Duca degli Abruzzi, 24, 10129 Torino, Italy.
E-mail address: carmine.todaro@polito.it (C. Todaro).

https://doi.org/10.1016/j.tust.2022.104756
Received 20 May 2022; Received in revised form 6 September 2022; Accepted 14 September 2022
Available online 2 October 2022

grout with the technical specifications (Càmara, 2018). However, the need for information related to these parameters faces the lack of suitable standard regulations for their reliable assessment. The main difficulties are related to the particular behaviour of two-component grout: it can be assimilated to a clay in the short term and to weak concrete (or hard soil) in the long term (Oggeri et al., 2021). This evolution is a function of the curing time (Todaro et al., 2021; Oreste et al., 2021) and the mix design, and can barely be framed from the available standards. Therefore, a unique, recognised method for the assessment of the elastic modulus is still not available at present, and has received little attention in the scientific literature (Mähner & Hausmann, 2017). Todaro et al. (2019) reported different charts related to UCS test for several mix designs of two-component grout and, although the elastic segment on the σ-ε curves was clearly recognizable also for short curing times, an analysis on the elastic parameters was not carried out. A last issue is the age of the two-component grout, which is of interest in tunnelling: short ages (up to 24 h) are undoubtedly the most important because in this time period the freshly cast grout is loaded with the weights of the linings that will form the newly assembled ring as the machine advances.

In the light of the above-mentioned situation, in this research the potential involvement of the bentonite in the elastic properties of two-component grout is investigated. A large test campaign focused on the elastic properties of two-component grout at short curing times was carried out by means of a geophysical approach. The procedure described in Todaro et al. (2020b) was followed and used as a comparison for the outcomes obtained. One typical mix design was selected and kept constant for all the test campaigns and 5 different bentonites were used. An additional mix design was completely scheduled without using bentonite. The results obtained provide evidence for the role of bentonite in the elastic properties of the grout. Furthermore, the orders of magnitude for the dynamic shear modulus (G), the dynamic Young's modulus (E), and the dynamic Poisson's ratio (ν) are provided and correlated with the experimental curves obtained from the investigation. These curves were interpolated by using a power law with three coefficients with 95 % confidence. The equations obtained are useful instruments that analytically summarise the obtained outcomes, i.e, the elastic parameters for a typical two-component grout mix design up to 24 h of curing.

2. General principles of two-component grout

Two-component grout is a cement-based technology characterised by two fluids that, once thoroughly mixed, give rise to a gelled material that starts instantaneously and continuously to harden (Hashimoto et al., 2005). The component A is a cement slurry, commonly made up of cement, bentonite and a retarder/fluidifying agent. However, in recent years new ingredients have also been used in the component A production to increase the strength and durability. Since studies on standard mortar can be considered forerunners for two-component grout, different innovative ingredients are now being tested (Li et al., 2021; Zhang et al., 2020), but the usage in two-component grouts is currently limited to ground blast furnace slag, fly ash, and metakaolin (Aboulayt et al., 2020; Andrè et al., 2022; Schulte-Schrepping and Breitenbücher, 2019; Song et al., 2020). The component B is a hardening accelerator, commonly composed of a silicate solution (Pellegrini and Perruzza, 2009). The mix design is expressly designed in order to guarantee a long workability and stability of the component A (commonly assessed by performing a bleeding test, as described in Wang et al. (2021) and Youn at al. (2016)), a gel time of the order of seconds and good mechanical properties in terms of strength and elastic properties. Both fluids run separately from the batching station, located outside the tunnel, to the injection nozzles located circumferentially on the shield tail. Here, only a few centimetres from the outlet of the nozzle into the annulus, the fluids are mixed and injected under pressure into the annulus (Hashimoto et al., 2005). From the mixing to the loss of fluidity of the obtained grout only a few seconds elapse and this time-lapse is defined as the gel time. After the gelation, the mechanical parameters start to increase continuously, reaching values that are a function of the mix design (Todaro et al., 2019).

Table 1
Mix design used.

	Ingredients	Dosage (kg/m^3)
Component A	Water	853
	Bentonite	30
	Portland Cement CEM I 52,5 R	230
	Retarding/fluidifying agent – Mapequick CBS1	3.5
Component B	Accelerator - Mapequick CBS3	81

Table 2
Chemical properties of the used cement (Cement CEM I 52,5 R).

Parameter	Test method	Indicative values
Sulphates (SO_3)	UNI EN 196/2	<3.7 %
Chlorides (Cl -)	UNI EN 196/2	<0.08 %
Loss on ignition	UNI EN 196/2	<5.0 %
Insoluble residue	UNI EN 196/2	<1.0 %
Water-soluble chromium VI	UNI EN 196/10	≤ 2 ppm

Table 3
Physical/mechanical properties of the used cement (Cement CEM I 52,5 R).

Parameter	Test method	Indicative values
Blaine specific surface area	EN 196/6	4000–5500 cm^2/g
Initial setting time	EN 196/3	>90 min
Volume stability	EN 196/3	≤10 mm
Flow test	UNI 7044	>70 %
Compressive strength after curing for	EN 196/1	
2 days		>35.0 MPa
28 days		>56.0 MPa

3. Material used and component a production

The mix design taken as the reference to produce two-component grout is reported in Table 1.

From this cornerstone, 6 different mix designs were created by changing the bentonite type (5 mix designs obtained) and removing it (1 mix design obtained). In this last case, the weight left by the bentonite was filled with water, according to the most common technique used to compile a two-component grout mix design. The difference in the water/cement ratio (w/c) with respect to the usage of the bentonite is equal to 10 kg/m^3. According to EFNARC (2005), this difference of 1.1 % in the dosage of the water does not affect the w/c and it can be considered that all the studied mixes are characterised by the same w/c. Indeed, the threshold value of tolerance in the metering phase of construction sites is ± 2 %. Irrespective of the considered mix design, the gel time ranges between 5 and 8 s.

Concerning the used cement, it contains at least 95 % of clinker and up to 5 % of minor constituents, that do not include the addition of calcium sulphate and additives. Further chemical and physical/mechanical information are reported in Table 2 and in Table 3.

Pertaining to the used bentonites, the prevalent adsorbed cation is Na^+ for all of them. The unit weight range is 2.5 – 2.7 kg/L. The swell index, a parameter that can simply characterise the aptitude of a certain bentonite to swell when it interacts with water (Lee and Shackelford, 2005), was experimentally assessed according to ASTM D5890-18. The X-ray diffraction analysis (XRD) was performed in order to characterise the used bentonites. The XRD technique is based on the observation of the scattered intensity of an X-ray beam, which is directed toward the sample, interact with it and produces a diffracted ray as a function of the incident and diffraction angle, of the polarization, and of the wavelength or energy. The outcomes for our samples (XRD tracks) are reported in

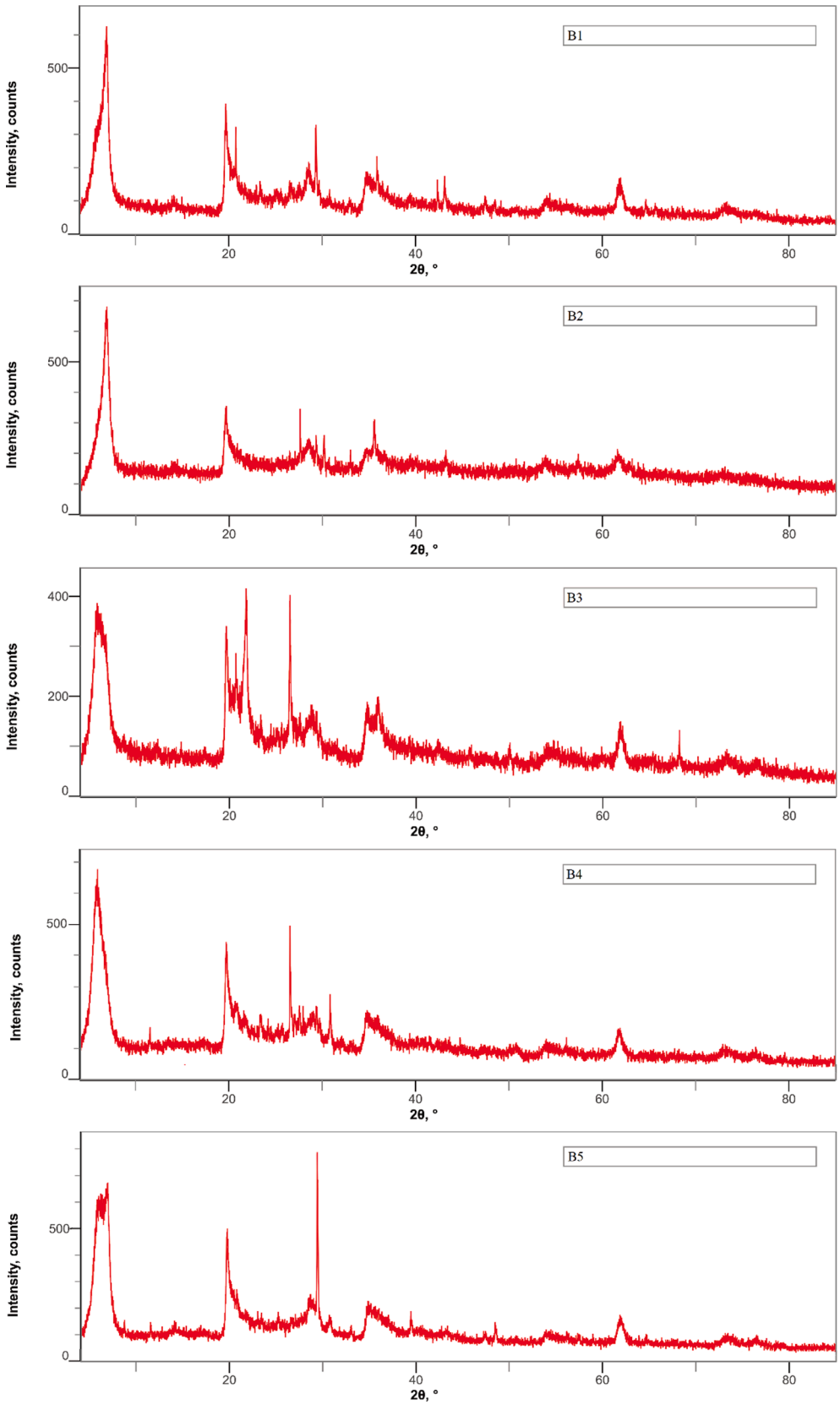

Fig. 1. XRD tracks of the used bentonites.

Table 4
Details of the six different mix designs: the name, the bentonite picture and the swell index (SWI).

Name of the mix	Bentonite pictures	Smectite content (% by weight)	SWI (ml/g)
B1		92	23
B2		98	13
B3		88	14
B4		94	12.7
B5	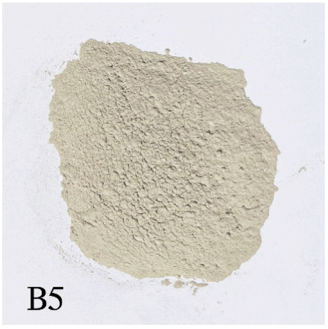	72	19.7
B-less	/		/

Table 5
Component A laboratory procedure, impeller speed and duration of the mixing step.

Operation	Impeller rotation speed (rpm)	Duration (min)
Fill the tank with water and start the mixer	800	/
Add the bentonite, increasing the propeller	from 800 to 2000	0.5
speed at a constant rate (bentonite	2000	6.5
activation)		
Add the cement	2000	3
Add the retarding/fluidifying agent	2000	2

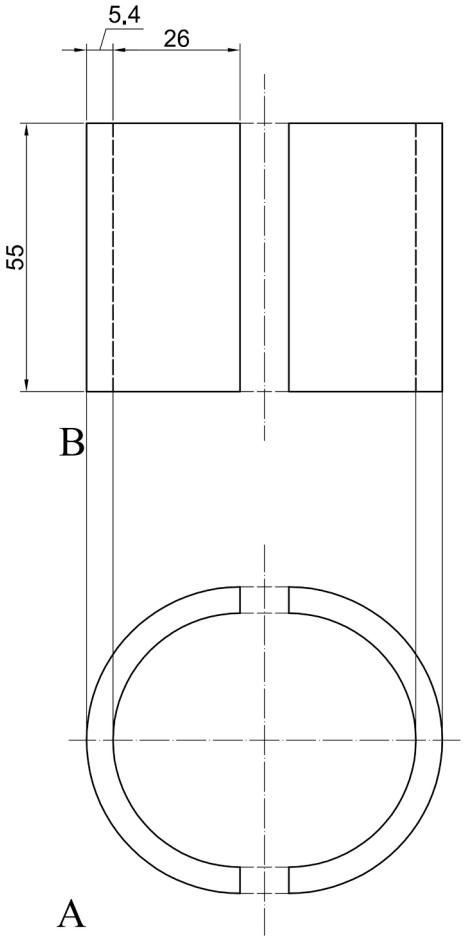

Fig. 2. Scheme of the used mould. All measures are expressed in mm. The two halves, before the casting, are linked together. A: orthogonal section; B: vertical section.

Fig. 1, showing the intensity of the signal as a function of the incidence angle. The analysis of the XRD tracks has permitted to estimate the percentage by weight of the smectite, a useful data often used for characterise bentonites (Dominijanni et al, 2019). For commercial reasons, the complete mineralogical distribution, and the relative mineralogical abundance have not been reported.

Table 4 reports the name of the mix designs, the bentonite pictures, the swell index (SWI) and the smectite percentage. "B-less" indicates the mix design without bentonite.

The component A was produced in the laboratory using a laboratory stirrer equipped with an impeller, according to the procedure described in Todaro et al. (2019). The duration of each mixing step is reported in Table 5.

The B-less mix design had an overall mix duration of only 5 min because of the lack of bentonite. Sample casting was performed

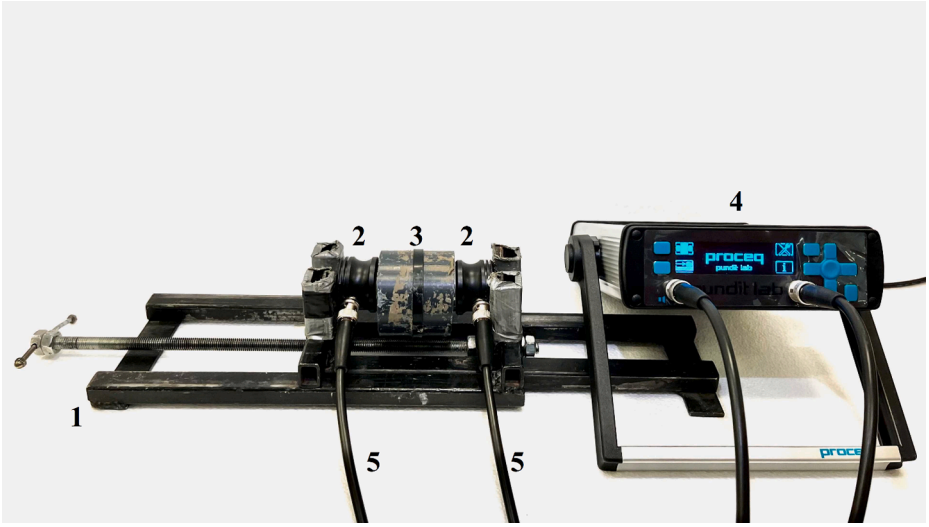

Fig. 3. The apparatus for the experimental measures. On the left, the holder bench (1) is the base support; the 250-kHz shear-wave transducers (2) are coupled to the sample, which is hold in the PVC mould (3). On the right, the Pundit Lab® instrument (by Proceq) (4) consists of a pulse generator, a receiver amplifier, and a time-measuring circuit. The Pundit Lab® is connected to the transducers via BNC cables (5).

according to Todaro et al. (2020a) and the sample shape was cylindrical, with dimensions chosen according to CEN (2004). The moulds were made up of two halves (coupled before the casting) obtained by tube of PVC PN 16 with an internal diameter of 52 mm and thickness of 5.4 mm (the PVC density ranged between 1.35 and 1.46 kg/l). The scheme is reported in Fig. 2.

The height was chosen as 55 mm (i.e., half of that described in the test campaign by Todaro et al. (2020b)) in order to minimise as much as possible the presence of air bubbles trapped in the grout (longer samples were tested and discarded because during the gelation the air bubbles inevitably remained trapped in the grout). All the sample casts were characterised by 2 perfectly flat bases and the transducer coupling pressure was calibrated for each assessment in order not to exceed the surface compression strength (SCS) (Todaro et al., 2020a) of the tested grout, in relation to the tested curing time. The density of the grout, irrespective of the mix design and curing time used, was kept constant at 1.204 kg/l. This assumption was confirmed realistic after a trial phase aimed at assessing the density value of the grout for each mix design. It was found that no differences were appreciable if the kind of bentonite changed since all values were averagely close to 1.204 kg/l. As concerns the curing condition, the samples were tested in a watertight condition, because they were protected by the mould on the lateral surface and covered by the transducers on the cylinder bases.

A preliminary test phase was performed to verify the possible influence of the casing on the results. After some laboratory tests, it was observed that the outcomes were not affected by the mould presence.

4. Methods

4.1. The UPV test

The ultrasonic pulse velocity (UPV) method is commonly adopted to assess the properties of hard concrete, such as elasticity and strength, to detect potential voids and cracks (Domone and Casson, 1997; Khan et al., 2011; Sturrup et al., 1984) and when a fresh grout is considered, to determine the rheological properties of cement-based grouts directly in-line (Rahman & Håkansson, 2013; Rahman et al., 2017). This non-destructive geophysical method is of pivotal importance if core sampling of existing concrete elements is not possible (Crawford, 1997; McCann and Forde, 2001; Popovics, 2003) or if the physical parameters of new concrete-based materials are unknown (e.g., Park et al., 2019; Todaro et al., 2020b). The UPV method is based on the propagation of longitudinal vibration pulses through rock materials and then on the measurement of the pulse velocities of the first-arrival elastic waves (longitudinal and shear waves). At the laboratory scale, an ultrasonic pulse is forced to propagate through a specimen (usually with a cylindrical shape) from an electro-acoustic transducer (the transmitter), which is placed in contact with one surface of the specimen, to another transducer (the receiver) placed on the opposite side. The pair of transducers usually have a central frequency of 54 kHz and a natural frequency ranging from 100 to 250 kHz. Once the ultrasonic pulse is detected by the receiver, the travelling time is measured and the ultrasonic velocity is easily calculated because the transmitter–receiver distance is known. The ultrasonic pulses depend on the density and elastic properties of the material (Aydin, 2013).

The velocities of the first arrival of the longitudinal P-wave (V_p) and of the transverse S-wave (V_s) are calculated to finally retrieve the dynamic mechanical properties of the investigated material. Given its density (ρ), the following equations (1) – (4) were adopted to estimate the shear modulus (G), the bulk modulus (K), the dynamic Poisson's ratio (ν) and the elastic modulus (E):

$$G = \rho V_s^2 \tag{1}$$

$$K = \rho V_p^2 - \frac{4}{3}G \tag{2}$$

$$\nu = \frac{V_p^2 - 2V_s^2}{2V_p^2 - 2V_s^2} \tag{3}$$

$$E = 2G(1+\nu) \tag{4}$$

Equations (1) – (4) should be corrected if the constrained condition occurs. Anyway, we experimentally proved that due to a minimal shrinkage phenomenon, an infinitesimal gap between the sample and the mould avoided the constrained condition.

This observation was also proved by preliminary test campaigns, performed by UPV tests on samples with and without moulds: the first arrival of the waves was exactly the same, proving that the mould did not affect the system. Therefore, we adopted the mould in all the laboratory tests. The above-reported equations were hence used for the computation. It should be signaled that if different types of mould are used (i.e., deformable moulds), the correspondence between results obtained with and without moulds should be preliminarily verified since it is not guaranteed. It is worth mentioning that the density of the

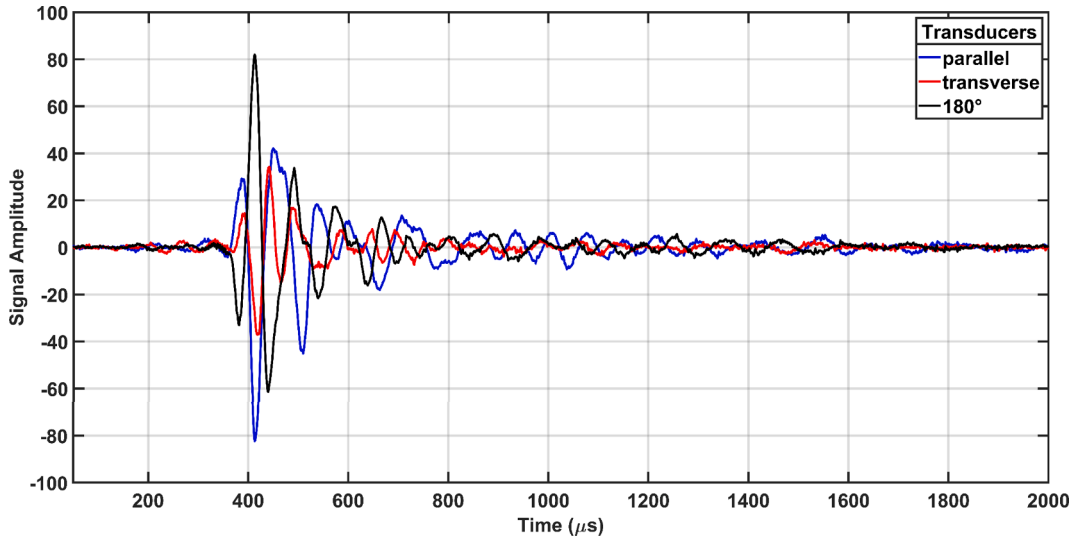

Fig. 4. Typical seismogram for signal acquired by varying the angle between the two transducers from 0° (blue line) to 90° (red line) to 180° (black line) in order to accurately detect the S-wave first arrival. This signal is of the B5 two-component grout at 6 h of curing time and the S-wave first arrival is at around 367 μs. (For interpretation of the references to colour in this figure legend, the reader is referred to the web version of this article.)

material should be accurately determined since it influences the calculation of the dynamic moduli. Moreover, these dynamic parameters are expected to differ from the static ones derived from loading experiments (Philleo, 1955; Lee et al.,1997; Agrò et al., 2009; Todaro et al., 2022a).

4.2. Experimental measures

The UPV tests were carried out using the instrument Pundit Lab® (manufactured by Proceq), which complies with the following standards: EN 12504–4 (Europe), ASTM C597-02:2016 (North America), BS 1881 Part 203:1986 (UK), ISO 1920-7:2004 (International), IS 13311:1992 (India), and CECS21:2000 (China). The device was connected via a USB to the power supply and to a laptop for the visualisation and saving of the measurements. Pundit Lab® comprises a pulse generator, receiver amplifier and a time-measuring circuit. A pair of 250 kHz shear wave transducers were connected to the device via BNC cables.

The transducers and the specimen were placed in a specific apparatus (Fig. 3), composed of a holder bench and a rotating handle that applied compression stress to the two free surfaces of the cylindrical specimen. The applied pressure was not a unique value for all the test campaign, but it was calibrated for each assessment performed, in function of the curing time and of the used mix design. For each test, in fact, the coupling pressure was selected as the maximum one applicable without damaging the sample. Practically, during the manually increasing of the pressure, a careful observation phase was carried out, focused on the transducers in contact with the grout. When water drops started to appear (bleeding water) on the edge transducers-grout, this was considered a clear warning of an applied pressure close to SCS. Consequently, the increasing of the pressure was interrupted and the geophysical measurement was acquired. This apparatus has been successfully adopted to ensure uniform and controlled conditions for the test and hence consistent results (Todaro et al., 2020b; Zarei et al., 2019), but it should be reported that a certain level of experience is required to select the contact pressure able to provide signals of high quality. In fact, if from one side the observation of small drops of water indicates a contact pressure close to the SCS (that should mean an excellent coupling and consequently a very good signal quality), it should be remembered that a layer of water can negatively affect the signal. A trial phase for the selection of the contact pressure is suggested, by continuously checking the signal quality with the Pundit Lab®. Providing some reference values, according to ISRM (1977), the applied pressure was about 0.3–0.4 MPa for the shortest curing time.

The excitation voltage was 500 V (the maximum allowed by our instrument). The receiver gain was either 10x or 100x, depending on the detected signal, which changed a lot as a function of the curing time of the two-component grout. An external amplifier (1 – 10 dB) was occasionally used if the signal was too weak to be detected at the early stages of curing (up to 3 h from casting). The time frame was 5 ms at the beginning of the tests and 1 ms after 2 h from casting.

Before the measurements, the Pundit Lab® was zeroed by means of the calibration of the transducers. They were put on both sides of the 25 μs calibration rod. A specific coupling gel was applied homogeneously to ensure no air was trapped between the transducer and the calibration rod. For the tests with the two-component grouts, the same gel was applied on the 250 kHz transducers. This non-toxic, water-soluble organic substance has high viscosity that allows shear waves to be properly transmitted into the grout. A good coupling between the transducer and the specimen is a condition for an accurate estimation of the UPV (Aydin, 2014).

During the measurements, the S-wave transducers were perfectly aligned in order to ensure a correct picking of the S-wave first arrival. In fact, S-waves are generated in a single plane and when the two transducers are orthogonal (90°) or misaligned the signal disappears or attenuates. A further check on the S-wave first arrival was done by rotating the parallel S-wave transducers from 0° to 180°. These two waveforms have the same first arrival and a very strong S-wave component, but they are opposite in phase. An example of this is shown in Fig. 4, where the signal acquired with 0°-aligned transducers is plotted in blue while that acquired with 180°-aligned transducers is plotted in black. The S-wave is strongly attenuated when the transducers are orthogonal (red line). This procedure was constantly applied for each S-wave measurement.

The first inspection of the waveforms was conducted on a laptop running the software Pundit Link. The recording was semi-automatic thanks to the data logging mode. The geophysical parameters of the two-component grouts are known to be dependent on the curing time (Todaro et al., 2020b). Therefore, the V_p and V_s resulting from the ultrasonic frequency of 250 kHz were calculated at different time steps. The signal was recorded every 15 min for curing times between 0 and 3 h, every 30 min for curing times between 3.5 and 6 h, and every 60 min for curing times between 7 and 26 h. The short curing time was densely recorded because it is of crucial importance in field operations. The record was composed of five readings per event, that is, five measurements at a time. The total number of recorded traces was between 139

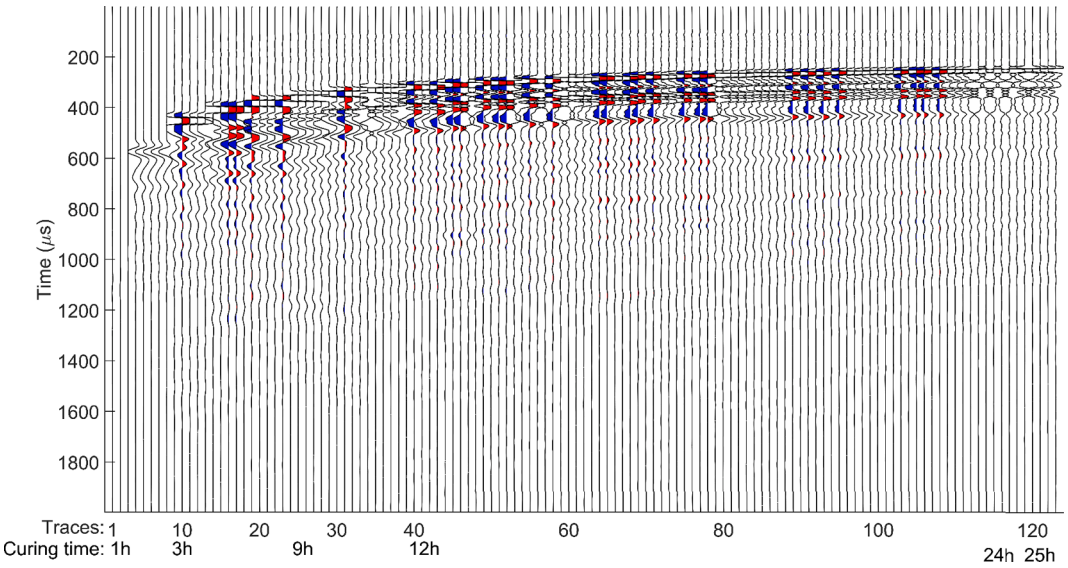

Fig. 5. The seismograms of 123 traces at different curing times (from 1 to 25 h after casting) for B5 grout. The first arrival times for V_p and V_s can be recognised. The signal highlighted in blue and red refers to the S-waves. The B5 grout was chosen as the representative grout as the other seismograms were quite similar. (For interpretation of the references to colour in this figure legend, the reader is referred to the web version of this article.)

Table 6
The values of V_s, ν, G, and E at 1 h from casting for the five two-component grouts (B1 - B5) and the grout without bentonite (B-less).

1 h from casting				
Grout	**V_s (m/s)**	**Poisson's ratio (ν)**	**G (MPa)**	**E (MPa)**
B1	43.2	0.4997	2.3	7.0
B2	46.4	0.4994	2.6	7.8
B3	30.6	0.4998	1.1	3.4
B4	36.0	0.4997	1.6	4.7
B5	52.5	0.4994	3.3	10.0
B-less	31.6	0.4997	1.1	3.4

Table 7
The values of V_s, ν, G and E at 24 h from casting for the five different two-component grouts (B1 - B5) and the grout without bentonite (B-less).

24 h from casting				
Grout	**V_s (m/s)**	**Poisson's ratio (ν)**	**G (MPa)**	**E (MPa)**
B1	253.4	0.4770	77.4	228.7
B2	278.9	0.4892	93.8	279.4
B3	250.0	0.4767	75.4	222.6
B4	248.8	0.4708	74.7	219.6
B5	257.9	0.4803	80.2	237.5
B-less	198.4	0.4843	44.9	133.2

(grout B2) and 187 (grout B4).

At the end of the tests, the acquired data were exported to be processed and analysed in Matlab. The travel time analysis was accomplished by manual picking of the first arrival time of V_p and V_s for each recorded trace.

5. Results

The seismogram in Fig. 5 represents the traces recorded for the two-component grout B5. It has been chosen as an example since the seismograms of the other grouts were quite similar. The first arrival of the S-waves can be easily recognised by the signal highlighted in blue and red (it ranges from 1000 μs at 1 h from casting to 200 μs at 25 h from casting). The first arrival of the P-waves is not reported in Fig. 5 because of difficulties in graphical representation due to strong differences of the wave intensity and first arrival.

However, irrespective of the mix design, the P-waves exhibited a quite constant trend over time ranging from 50 μs (for B4) to 40 μs (for B5 and B-less) and 30 μs (for B1, B2, B3). Since the slight variation on the first arrival time (in the range of few μs) would have minimally influenced the value of the moduli (which is mostly influenced by V_s), a constant value of V_p for each grout was used for the subsequent computations.

Once the arrival times were picked, the following parameters were calculated for each grout: V_p, V_s ν, G, and E. The bulk modulus K was not included in this study since it is not required by the stakeholders in the field of two-component grouts. The computed values are listed in Table 6 for 1 h of curing time and in Table 7 for 24 h of curing time.

The comparative plots in Fig. 6 allow the visualisation of the behaviour of the six grouts with time: B1 (dotted line), B2 (circles and solid line), B3 (dash-dotted line), B4 (triangles and solid line), B5 (dashed line) and B-less (red solid line). The S-wave velocity is plotted in Fig. 6a) and increases with time with a similar trend for all the grouts, except for B-less that increases at a slower rate. The Poisson's ratio (Fig. 6 b) slightly decreases from 0.5 to 0.48 (B2, B3, B-less) or to 0.47 (B1, B4, B5) during the 1-day of hardening. All the grouts show increasing values of E and G with time (Fig. 6 c and d, respectively).

6. Final remarks/comments

Taking into account Fig. 6 as a whole, it jumps out at readers that no curves start from time zero. This issue was unavoidable due to mechanical limitations because, even though the two-component grout had completed its gelation process, the material was too weak to guarantee a good transducer coupling before 45–60 min of curing (SCS around 0.4 MPa that yields a UCS of about 0.1 MPa – Todaro et al. (2020a)). It should be reported that only two grouts (B4 and B-less) allowed a good signal recording at 30 min of curing time with no damage to the sample-transducer interface. Moreover, it is worth mentioning that it is impossible to detect the S-waves at the shortest curing times due to the large amount of water (w/c $\simeq$ 3.71) that, after the gelation, is still not involved in the hardening reaction in the specimen. S-waves do not propagate in water. As the hardening process of cement starts, the free water gets involved in the hardening reaction, allowing the detection of the S-wave arrival. Another comment regards the increasing trend of the S-waves: the first arrival of the S-wave considerably decreases in the 12

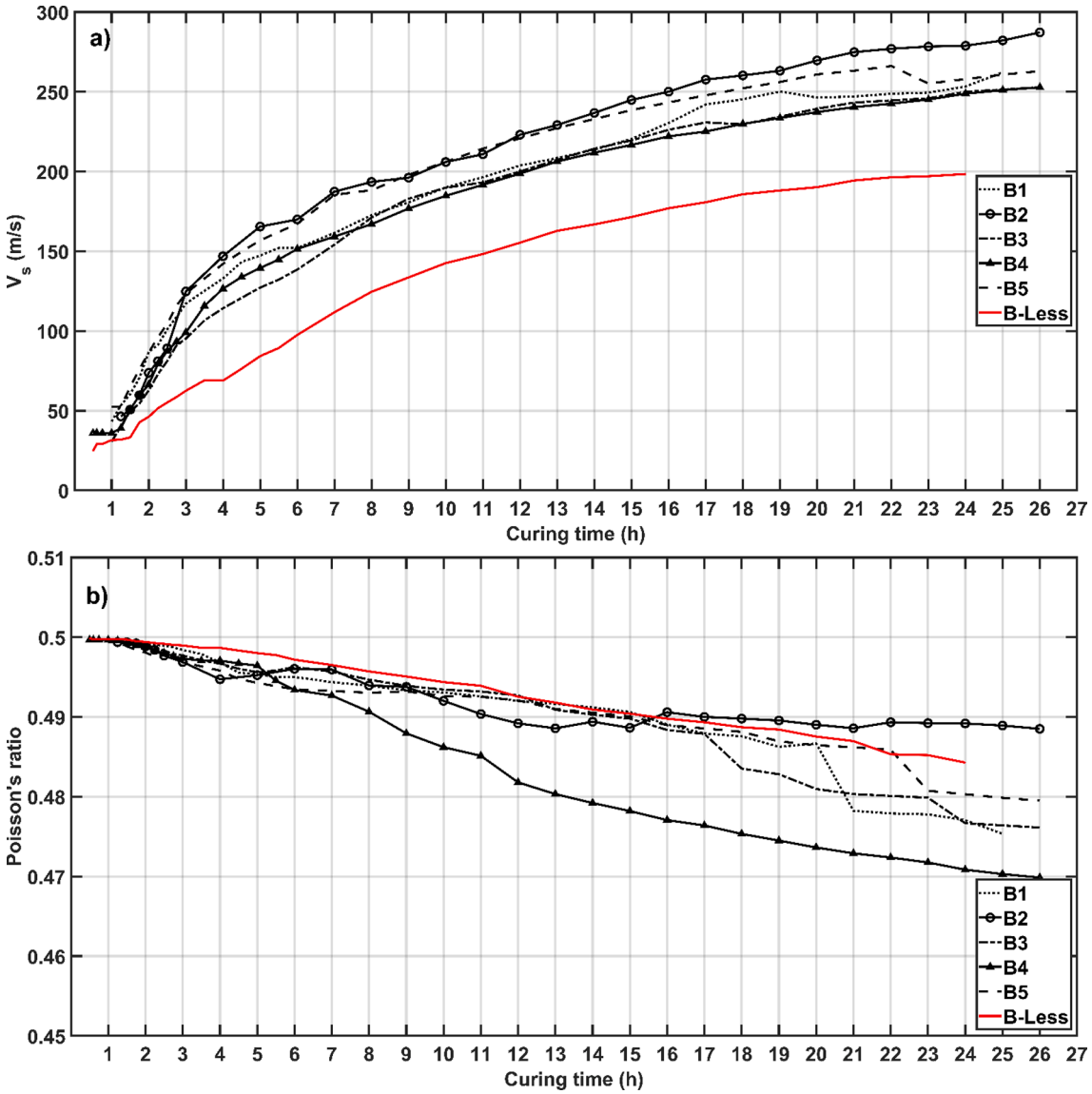

Fig. 6. Comparison of the four computed parameters: a) S-wave velocity (V_s), b) Poisson's ratio (ν), c) elastic modulus (E), d) shear modulus (G) for the two-component grouts B1 (dotted line), B2 (circles and solid line), B3 (dash-dotted line), B4 (triangles and solid line), B5 (dashed line) and B-less (red solid line). (For interpretation of the references to colour in this figure legend, the reader is referred to the web version of this article.)

h after the casting and then becomes stable. In fact, after 12 h of curing, a percentage between 75 and 80 of the maximum value of V_s is reached, irrespective of the mix design. Considering Fig. 6 a), it can be observed that the range of V_s is between 31 m/s (B3) at short times and 279 m/s (B2) at long times. Furthermore, it can be easily recognised that, irrespective of the curing times, the grout without bentonites (B-less) has the lowest V_s throughout the 24 h. It can then be concluded that the use of the bentonite in the mix design results in an increment of V_s ranging between 25 % and 80.5 % with respect to the B-less. This remark is very important since it proves the engagement of the bentonite in the hardening process of the two-component grout.

Pertaining to Poisson's ratio, Fig. 6b) can be analysed. Irrespective of the mix design, all curves started from a value of ν equal to 0.5 (the value characterising incompressible materials like water) for curing times close to 1 h. This finding matches the statement previously reported, i.e., the two-component grout for curing times shorter than 1 h has a behaviour controlled by the presence of water, rather than by the other ingredients of the grout. During the hardening, a reduction of ν is observed, reaching values ranging between 0.4708 and 0.4892 (related to B2 and B4, respectively) at 1 day of curing. B-less shows a trend above all the other curves up to 12 h, whereupon it reaches a value within the range reported above.

Concerning the elastic moduli E and G, Fig. 6 c) and d) can be inspected, respectively. At 1 day of curing time, the weakest moduli are for B-less, with $E < 150$ MPa and $G < 50$ MPa. All the other mix designs exhibited values higher than 219 MPa and 74 MPa for E and G, respectively. The use of the bentonite has a strong effect on both the moduli: an increment between 65 % and 110 % can be obtained by adding the bentonite to the mix design of the two-component grout. For completeness, the highest moduli recorded are developed by grout B2, with $E = 300$ MPa and $G = 100$ MPa at 26 h of curing time.

Similar inferences can be observed at lower curing times.

In light of the presented result, some comments related to the bentonite properties are due. Unfortunately, no dependence between the SWI and the elastic properties analysed can be spotted as well as the smectite content does not provide support in this task. Considering Fig. 6 and taking as reference B2 (that exhibited the highest values of E and G after 12 h of curing), it can be stated that this bentonite is characterised

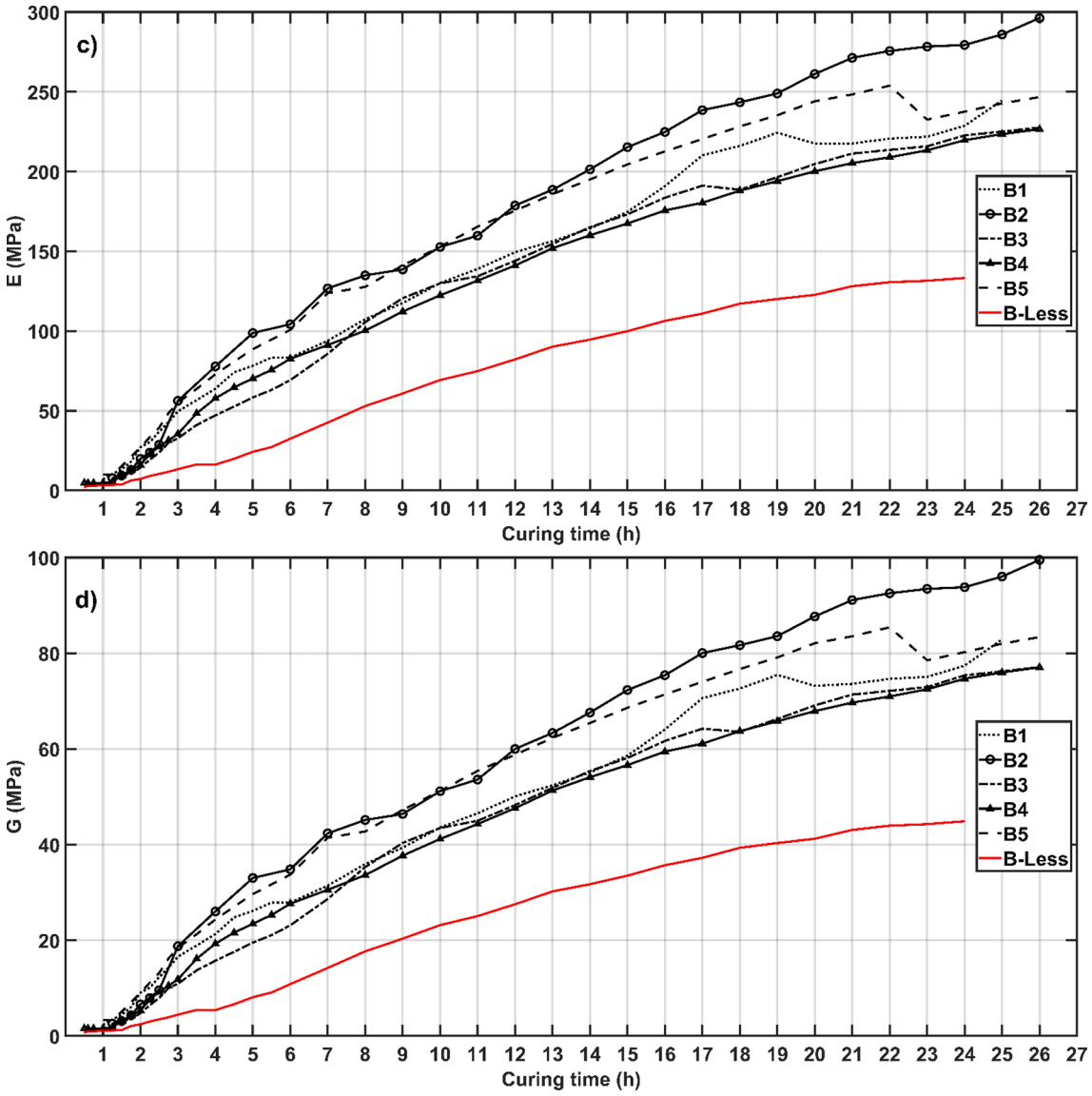

Fig. 6. (*continued*).

by the highest value of smectite content (98 % by weight), but this parameter cannot be taken as reference for choosing the best bentonite since for shorter curing times (<12 h) it behaves similarly to B5, that has the lowest smectite content of the used bentonite (72 %). Moreover, their relative SWI are different (13 and 19.7 ml/g, respectively). Similar conclusion can be obtained observing the behaviour of B1, B3 and B4, with approximately the same trend (Fig. 6 a, c and d) but different characterising parameters. In conclusion, it can be stated that at this moment a valuable parameter of the bentonite able for predicting the behaviour of the two-component grout has not been recognized. Probably, some additives commonly used for preparing commercial bentonites play an important role in the curing of the two-component grout. The practice of adding polymers to the bentonite for improving the stabilizing aptitude, for example, is quite common and how this practice affects the curing of the grout has not yet been investigated. The prevalent adsorbed cation does not provide useful information as well, since all the studied bentonites are sodic. Anyway, a general hypothesis can be advanced, pertaining to the general role played by bentonites in the elastic properties of a standard two-component grout compared to a grout prepared without bentonite (B-Less). In fact, it can be speculated that bentonite, due to its natural tendency to swell and to adsorb molecules of water, could slightly decrease the water/cement ratio, providing as effect an increasing of the moduli (as well as presumably an increasing of SCS), for a certain curing time, respect to the grout produced without bentonite.

Table 8
The coefficients of the power law that interpolates the V_s data for the five two-component grouts (B1 - B5) and the grout without bentonite (B-less). The R^2 of the interpolation is also provided.

Grout	a	b	c	R^2
B1	793.4	0.07589	−751.8	0.9951
B2	−2406.0	−0.03643	2424.0	0.9950
B3	853.8	0.07556	−832.4	0.9964
B4	224.1	0.20670	−179.0	0.9902
B5	−1953.0	−0.03907	1991.0	0.9949
B-less	55.1	0.45840	−25.1	0.9887

As the last step of the work, a further analysis of the V_s data was performed. In fact, considering the slight decreasing of the P-wave velocity for the studied curing time, irrespective of the mix design used, it has been assumed that the S-wave velocity mainly influences E, G and ν. Consequently, the V_s data were processed to find the fitting curves that best analytically explained them. The Curve Fitting Toolbox™ in Matlab

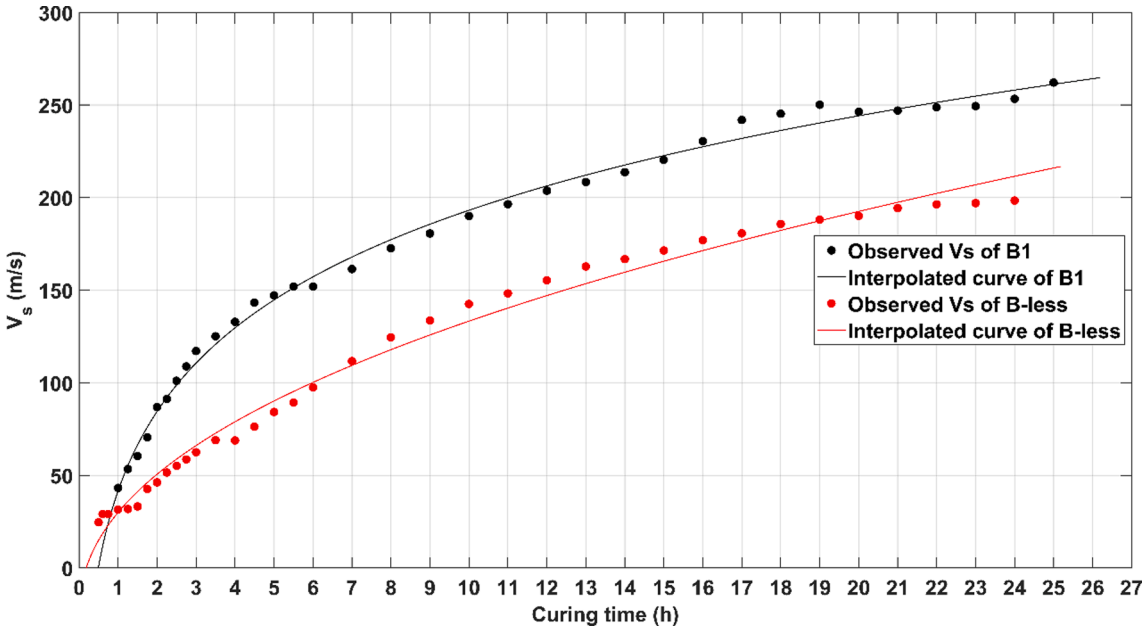

Fig. 7. The curve fitting of V_s for two representative grouts: B1 (black) and B-less (red). The observed velocity is plotted with dots and the interpolating power law calculated in Matlab is plotted with solid line. The coefficients of the power law are listed in Table 8. (For interpretation of the references to colour in this figure legend, the reader is referred to the web version of this article.)

was used for this purpose. The best interpolation of the experimental data was the power law with three coefficients:

$$V_s(t) = at^b + c \tag{5}$$

where t is the curing time in hours. The coefficients (with 95 % confidence bounds) and the R-square of the interpolations are listed in Table 8 for each grout. Fig. 7 represents the data fitting between the observed V_s and the interpolating analytical curve that follows the power law for two representative grouts: B1 and B-less.

This last analysis provides the parameters that allow the reconstruction of the experimentally obtained V_s curves following Equation (5). This could represent a valid tool for all the stakeholders involved in the two-component grout field since by using these parameters it is possible to reproduce the trends of V_s and obtain values of E, G and ν for any curing times ranging between 1 and 24 h. The provided outcomes are innovative: at the present time, the geophysical approach described in this work is the only able to provide numerical values pertaining to the elastic parameters of the two-component grout at short curing times (shorter than 24 h). If, on one side, the order of magnitude of the elastic parameters as a function of the studied curing time is precious for calibrate the numerical model, on the other side, the UPV method could be a valid method applicable also in construction sites, integrating it in testing protocol commonly adopted for assess the grout compliance with the technical specification. A last clarification is due: parameters provided in this work are "dynamic" and should not be confused with the "static" parameters (Todaro et al., 2022a).

7. Conclusions

This research was carried out in order to study the potential role of the bentonite in the elastic parameters of two-component grout at short curing times and to provide a reliable order of magnitude of the elastic parameters related to the curing times, this being of more interest for tunnelling engineers. In fact, at the present time, the scientific literature has recognised the role of the bentonite only in component A stabilisation and in the SCS at short curing times. In this paper, the geophysical UPV technique made it possible to highlight the role of the bentonite also in the elastic parameters of the hardening grout. Irrespective of the bentonite used (B1 – B5), considerable increments of E and G were recognised with respect to the grout without the bentonite (B-less). The bentonite's influence on the Poisson's ratio was less than on the dynamic moduli, even though ν for B-less is larger than the others up to 12 h. Having recognised V_s as the main parameter of the study (because V_p decreased minimally for the analysed curing times), the power-law interpolation performed in Matlab provided the specific analytical equations of the six mix designs. This outcome represents a very useful tool for all the stakeholders involved in the two-component grout field, since it makes it possible to forecast the elastic parameters of the two-component grout for any times ranging between 1 and 24 h.

According to the author's knowledge, this is the first work that highlights the influence of bentonite on the elastic parameters of the two-component grout. This influence could be due to the aptitude of bentonite to swell, causing a slight reduction of the water-cement ratio and consequently an increasing of the mechanical performances. To date, it is not possible to unequivocally predict the elastic parameters of a two-component grout as a function of a certain specific bentonite. The typology of the prevalent adsorbed cation seems not to have a strong effect, as well as the smectite content. This issue, for a given mix design (fixed dosages), could depend on the chemical composition of the bentonite, since some special polymers/additives are often added to the clay powder in order to improve the required characteristics. Unfortunately, the potential presence of these added polymers is still undetectable if common tests for the characterisation, such as the SWI, are adopted.

CRediT authorship contribution statement

Carmine Todaro: Conceptualization, Methodology, Validation, Investigation, Resources, Writing – original draft, Writing – review & editing, Visualization. **Francesca Pace:** Conceptualization, Methodology, Data curation, Software, Formal analysis, Resources, Writing – review & editing.

Declaration of Competing Interest

The authors declare that they have no known competing financial

interests or personal relationships that could have appeared to influence the work reported in this paper.

Acknowledgements

The research activity of F. Pace is funded by the NOP Research and Innovation 2014-2020, Axis IV "Education and research for recovery – REACT-EU". The authors want to thank Prof. Alberto Godio and Prof. Daniele Peila for their valuable suggestions and support during the research. Further thanks go to Aarathy Ezhuthupally Reghuprasad for helping during the preliminary part of the test campaign. Special thanks also to Utt Mapei for providing materials for the grout production.

Funding

This research did not receive any specific grant from funding agencies in the public, commercial, or.
not-for-profit sectors.

References

Aboulayt, A., Souayfan, F., Roziere, E., Jaafri, R., Cherki El Idrissi, A., Moussa, R., Justino, C., Loukili, A., 2020. Alkali-activated grouts based on slag-fly ash mixtures: From early-age characterization to long-term phase composition. Constr. Build. Mater. 260 (2020), 120510 https://doi.org/10.1016/j.conbuildmat.2020.120510.

Agrò, G., Lo Giudice, E., Sacco, M.M. 2009. Il modulo elastico statico e dinamico del calcestruzzo. In Proceedings of "Conferenza Nazionale AIPnD - Prove non Distruttive Monitoraggio Diagnostica", Roma (IT), October 19.

André, L., Bacquié, C., Comin, G., Ploton, R., Achard, D., Frouin, L., Cyr, M., 2022. Improvement of two-component grouts by the use of ground granulated blast furnace slag. Tunn. Undergr. Sp. Tech. 122, 104369 https://doi.org/10.1016/j.tust.2022.104369.

ASTM C597-02, 2016. Standard Test Method for Pulse Velocity Through Concrete, American Society for Testing and Material International.

ASTM D5890, 2018. Standard Test Method for Swell Index of Clay Mineral Component of Geosynthetic Clay Liners, American Society for Testing and Material International.

Aydin, A., 2014. Upgraded ISRM suggested method for determining sound velocity by ultrasonic pulse transmission technique. Rock Mech. Rock Eng. 47, 255–259. https://doi.org/10.1007/s00603-013-0454-z.

Boscaro, A., Barbanti, M., Dal Negro, E., Plescia, E., Alexandrowicz, M., 2015. The first successful experience in Poland of tunnel excavation with EPB for the Metro Warsaw. In: Proceedings of the ITA WTC World Tunnel Congress 2015, Dubrovnik (HR), May 22-28.

BS 1881-203, 1986. Testing concrete. Recommendations for measurement of velocity of ultrasonic pulses in concrete, British Standards Institution.

Càmara, R.J., 2018. Use of two-component mortar in the precast lining backfilling of mechanized tunnels in rock formations. In: Proceedings of the ITA WTC World Tunnel Congress 2018, Dubai (UAE), April 20-26.

CECS21, 2000. Technical specification for inspection of concrete defects by ultrasonic method, China Association for Engineering Construction Standardization Committee of the concrete structure.

CEN, 2004. Testing concrete. Determination of ultrasonic pulse velocity. EN 12504–4: 2004. European Committee for Standardization, Brussels (B).

Crawford, G.I., 1997. Guide to Nondestructive Testing of Concrete. Technical Report No. FHWA-SA-97-105; U.S. Department of Transportation: Washington, DC, USA, 1997, 44–52.

Dominijanni, A., Fratalocchi, E., Guarena, N., Manassero, M., Mazzieri, F., 2019. Critical issues in the determination of the bentonite cation exchange capacity. Géotech. Lett. 9 (3), 205–210.

Domone, P.L., Casson, R.B.J., 1997. Ultrasonic testing of concrete. NDT E Int. 1997 (4), 265.

EFNARC, 2005. Specification and guidelines for the use of specialist products for mechanised tunnelling TBM in soft ground and hard rock. European Federation of National Associations Representing for Concrete, Flums (CH).

Hashimoto, T., Brinkman, J., Konda, T., Kano, Y., Feddema, A., 2005. Simultaneous Backfill Grouting, Pressure Development in Construction Phase and in the Long-Term. Tunnelling. A Decade of Progress. GeoDelft 1995-2005. Adam Bezuijen, Haike van Lottum, CRC Press.

IS 133311, 1992. Method of Non-destructive testing of concret, Part 1: Ultrasonic pulse velocity [CED 2: Cement and Concrete]. BUREAU OF INDIAN STANDARDS.

ISO 1920-7, 2004. Testing of concrete — Part 7: Non-destructive tests on hardened concrete, International Organization for Standardization.

Isrm, 1977. Suggested methods for determining sound velocity. Technical Report. International Society for Rock Mechanics: Commission on Standardization of Laboratory and Field Test.

Ivantchev, A., Del Rio, J., 2015. Two-component backfilling grouting for double shield TBMs. In: Proceedings of the ITA-AITES World Tunnel Congress 2015. Dubrovnik (HR), May 22–28.

Khan, Z., Cascante, G., Hesham El Naggar, M., 2011. Measurement of dynamic properties of stiff specimens using ultrasonic waves. Can. Geotech. J. 48, 1–15. https://doi.org/10.1139/T10-040.

Lee, K.-M., Kim, D.-S., Kim, J.-S., 1997. Determination of dynamic Young's modulus of concrete at early ages by impact resonance test". J. Civi. Eng. 1, 11–18.

Lee, J.M., Shackelford, C.D., 2005. Solution retention capacity as an alternative to the swell index test for sodium bentonite. Geotech. Test. J. 28 (1), 61–70. https://doi.org/10.1520/GTJ12520.

Li, S., Zhang, J., Li, Z., Liu, C., Chen, J., 2021. Feasibility study on grouting material prepared from red mud and metallurgical wastewater based on synergistic theory. J. Hazard. Mater. 407, 124358 https://doi.org/10.1016/j.jhazmat.2020.124358.

Mähner, D., Hausmann, M., 2017. New Development of an Annular Gap Mortar for Mechanized Tunnelling. In: Proceedings of the AFTES International Congress 2017, Paris (FR), November 13-16.

McCann, D.M., Forde, M.C., 2001. Review of NDT methods in the assessment of concrete and masonry structures. NDT&E Int. 34, 71–84. https://doi.org/10.1016/S0963-8695(00)00032-3.

Mesboua, N., Benyounes, K., Benmounah, A., 2018. Study of the impact of bentonite on the physico-mechanical and flow properties of cement grout. Cogent Eng. 5 (1), 1446252. https://doi.org/10.1080/23311916.2018.1446252.

Oggeri, C., Oreste, P., Spagnoli, G., 2021. The influence of the two-component grout on the behaviour of a segmental lining in tunnelling. Tunn. Undergr. Sp. Tech. 109, 103750 https://doi.org/10.1016/j.tust.2020.103750.

Oggeri, C., Oreste, P., Spagnoli, G., 2022. Creep behaviour of two-component grout and interaction with segmental lining in tunnelling. Tunn. Undergr. Sp. Tech. 119, 104216 https://doi.org/10.1016/j.tust.2021.104216.

Oreste, P., Sebastiani, D., Spagnoli, G., de Lillis, A., 2021. Analysis of the behavior of the two-component grout around a tunnel segmental lining on the basis of experimental results and analytical approaches. Transport. Geotech. 29, 100570 https://doi.org/10.1016/j.trgeo.2021.100570.

Park, J.Y., Yoon, Y.G., Oh, T.K., 2019. Prediction of concrete strength with P-, S-, R-wave velocities by support vector machine (SVM) and artificial neural network (ANN). App. Sci. 9 (19), 4053.

Peila, D., Borio, L., Pelizza, S., 2011. The behaviour of a two-component backfilling grout used in a tunnel-boring machine. Acta Geotech. Sloven. 8, 5–15.

Pelizza, S., Peila, D., Borio, L., Dal Negro, E., Schulkins, R., Boscaro, A. 2010. Analysis of the performance of two-component back-filling grout in tunnel boring machines. In Proceedings of the ITA World Tunnel Congress, WTC 2010, Vancouver (CA), May, pp.14–20.

Pelizza, S., Peila, D., Sorge, R., Cignitti, F. 2011. Back-fill grout with two component mix in EPB tunneling to minimize surface settlements: Roma Metro – line C case history, Geotechnical Aspects of Underground Construction in Soft Ground, International Symposium on Geotechnical Aspects of Underground Construction in Soft Ground, held in Rome (IT), May 16–18.

Pellegrini, L., Perruzza, P., 2009. Sao Paulo metro project – control of settlements in variable soil conditions through EPB pressure and bicomponent backfill grout. US Society for Mining, Metallurgy, and Exploration. In: Proceedings of the 19th Conference of Rapid Excavation and Tunnelling, Las Vegas (USA), pp. 1137–1153.

Philleo, R.E., 1955. Comparison of results of three methods for determining Young's modulus of elasticity of concrete". J Am Concrete I. 51 (1), 461–469.

Popovics, J.S., 2003. NDE techniques for concrete and masonry structure. Progress in structural engineering and materials. Prog. Struct. Mat. Eng. 5, 49–59.

Rahman, M., Wiklund, J., Kotzé, R., Håkansson, U., 2013. In-line ultrasound based rheology - A new tool for the measurement of flow and rheological properties of cement based grout. In Proceeding of the 47th US Rock Mechanics / Geomechanics Symposium 2013, San Francisco, California (USA), June 201.

Rahman, M., Wiklund, J., Kotzé, R., Håkansson, U., 2017. Yield stress of cement grouts. Tunn. Undergr. Sp. Tech. 61, 50–60. https://doi.org/10.1016/j.tust.2016.09.009.

Schulte-Schrepping, C., Breitenbücher, R., 2019. Two-component grouts with alkali-activated binders. In: Proceedings of the ITA-AITES World Tunnel Congress 2019, Naples (IT), May 3–9.

Shah, R., Lavasan, A.A., Peila, D., Todaro, C., Luciani, A., Schanz, T., 2018. Numerical study on backfilling the tail void using a two-component grout. J. Mater. Civ. Eng. 30 (3) https://doi.org/10.1061/(ASCE)MT.1943-5533.0002175.

Song, W., Zhu, Z., Pu, S., Wan, Y., Huo, W., Song, S., Zhang, J., Yao, K., Hu, L., 2020. Synthesis and characterization of eco-friendly alkali-activated industrial solid waste-based two-component backfilling grouts for shield tunnelling. J. Clean. Prod. 266, 121974 https://doi.org/10.1016/j.jclepro.2020.121974.

Sturrup, V.R., Vecchio, F.J., Caratin, H., 1984. In: Pulse Velocity as a Measure of Concrete Compressive Strength, In-situ Non-destructive Testing of Concrete. American Concrete Institute, Detroit (USA), pp. 201–227.

Thewes, M., Budach, C., 2009. Grouting of the annular gap in shield tunneling – an important factor for minimisation of settlements and production performance. In: Proceedings of the ITA-AITES World Tunnel Congress 2009, Budapest (HU), May 23–28.

Todaro, C., Bongiorno, M., Carigi, A., Martinelli, D., 2020a. Short term strength behavior of two-component backfilling in shield tunneling: comparison between standard penetrometer test results and UCS. Geoing. Ambient. Miner. 159 (1), 33–40.

Todaro, C., Carigi, A., Martinelli, D., Peila, D., 2021. Study of the shear strength evolution over time of two-component backfilling grout in shield tunnelling. Case Stud. Constr. Mater. 15 (2021), e00689.

Todaro, C., Peila, L., Luciani, A., Carigi, A., Martinelli, D., Boscaro, A., 2019. Two component backfilling in shield tunneling: laboratory procedure and results of a test campaign. In: Proceedings of the ITA WTC World Tunnel Congress 2019, Naples (IT), May 3–9.

Todaro, C., Carigi, A., Saltarin, S., Peila, D., Cardu, M. 2022a. The two-component grout: a double approach for the Young's modulus assessment. In Proceeding of ITA-AITES World Tunnel Congress, WTC 2022, Copenhagen (DK), April 22–28.

Todaro, C., Godio, A., Martinelli, D., Peila, D., 2020b. Ultrasonic measurements for assessing the elastic parameters of two-component grout used in full-face mechanized tunnelling. Tunn. Undergr. Sp. Tech. 106, 103630 https://doi.org/10.1016/j.tust.2020.103630.

Todaro, C., Martinelli, D., Boscaro, A., Carigi, A., Saltarin, S., Peila, D., 2022b. Characteristics and testing of two-component grout in tunnelling applications. Geomech. Tunn. 15 (1), 121–131. https://doi.org/10.1002/geot.202100019.

Todaro, C., Saltarin, S., Cardu, M., 2022c. Bentonite in two-component grout applications. Case Stud. Constr. Mater. 16, e00901.

Viccaro, M., 2018. Doped bentonitic grouts for implementing performances of low-enthalpy geothermal systems. Geoth. Energy. 6, 4. https://doi.org/10.1186/s40517-018-0090-7.

Wan, Y., Zhu, Z., Song, L., Song, S., Zhang, J., Gu, X., Xu, X., 2021. Study on temporary filling material of synchronous grouting in the middle of shield. Constr. Build. Mater. 273, 121681 https://doi.org/10.1016/j.conbuildmat.2020.121681.

Wang, X., Li, S., Zhou, A., Liu, R., Duan, S., Wang, M., 2021. Influence of the bleeding characteristic on density and rheology in cement slurry. Constr. Build. Mater. 269, 121316 https://doi.org/10.1016/j.conbuildmat.2020.121316.

Youn, B., Schulte-Schrepping, C., Breitenbücher, R., 2016. Properties and Requirements of Two-Component Grouts in Mechanized Tunnelling. In: Proceedings of the ITA-AITES World Tunnel Congress 2016, San Francisco (USA), April 22–28.

Zarei, Y., Uromeihy, A., Reza Nikoodel, M., Fathollahy, M., 2019. A testing procedure for determining ultrasonic wave velocity. B. Geofis. Teor. Appl. 60, 433–442. https://doi.org/10.4430/bgta0272.

Zhang, J., Li, S., Li, Z., 2020. Investigation the synergistic effects in quaternary binder containing red mud, blast furnace slag, steel slag and flue gas desulfurization gypsum based on artificial neural networks. J. Clean. Prod. 273, 122972 https://doi.org/10.1016/j.jclepro.2020.122972.